processes

MDPI

Article

Systematic and Model-Assisted Process Design for the Extraction and Purification of Artemisinin from *Artemisia annua* L.—Part IV: Crystallization

Maximilian Johannes Huter, Axel Schmidt, Fabian Mestmäcker, Maximilian Sixt and Jochen Strube *

Institute for Separation and Process Technology, Clausthal University of Technology, 38678 Clausthal-Zellerfeld, Germany; Huter@itv.tu-clausthal.de (M.J.H.); Schmidt@itv.tu-clausthal.de (A.S.); Mestmaecker@itv.tu-clausthal.de (F.M.); Sixt@itv.tu-clausthal.de (M.S.)

* Correspondence: strube@itv.tu-clausthal.de; Tel.: +49-5323-72-2355

Received: 30 August 2018; Accepted: 26 September 2018; Published: 2 October 2018

Abstract: In this study, process integration for crystallization of a priori purified *Artemisia annua* L. is investigated. For this total process, the integration operation boundaries and behavior of the crystals are studied. This is performed focusing on a conceptual process design study for artemisinin, aiming towards the development of a crystallization step under given parameters by process integration. At first, different crystallization systems consisting of ethanol-water or acetone-water mixtures are compared. In subsequent steps, the metastable zone width and the behavior of the crystals regarding agglomeration and breakage are checked. Furthermore, the sensitivities of process variables based on several process parameters are investigated. Additionally, the final process integration of crystallization as a combined purification and isolation step is studied.

Keywords: artemisinin; conceptual process design; crystallization

1. Introduction

Highly purified substances from natural sources are used to treat various diseases. In addition, the social demand continues to rise [1,2]. To obtain pure substances from plant material, several process steps are necessary. A typical process may include extraction as a capture step, followed by purification steps such as liquid-liquid extraction, chromatography and crystallization [3–6].

The whole study includes a detailed investigation of each process step, a conceptual process design and cost estimation. These aspects are divided into the following five articles:

Part 0: Sixt, M.; Strube, J. Systematic and model-assisted evaluation of solvent based- for pressurized hot water extraction for the extraction of Artemisinin from *Artemisia annua* L. *Processes* 2017, 5, 86, doi:10.3390/pr5040086 [7].

Part I: Sixt, Schmidt et al. Systematic and model-assisted process design for the extraction and purification of Artemisinin from *Artemisia annua* L.—Part I: Conceptual process design and cost estimation. *Processes* 2018, 6, 161, doi:10.3390/pr6090161 [8].

Part II: Schmidt, Sixt et al. Systematic and model-assisted process design for the extraction and purification of Artemisinin from *Artemisia annua* L.—Part II: Model-based design of agitated and packed columns for multistage extraction and scrubbing. *Processes* 2018, 6, 179, doi:10.3390/pr6100179 [9].

Part III: Mestmäcker, Schmidt et al. Systematic and model-assisted process design for the extraction and purification of Artemisinin from *Artemisia annua* L.—Part III: Chromatographic Purification. *Processes* 2018, 6, 180, doi:10.3390/pr6100180 [10].

Part IV: Huter, Schmidt et al. Systematic and model-assisted process design for the extraction and purification of Artemisinin from *Artemisia annua* L.—Part IV: Crystallization. (this article).

A model-based optimization for the extraction step was performed in a previous study by the institute [7]. The general concept is based on the example of 10-deacetylbaccatin III, which is obtained from yew. The process flow sheet and the target component are depicted in Figures 1 and 2 [6]. A detailed process description and a summary of properties are given in Part 1 This article focusses on the crystallization step of this conceptual process design.

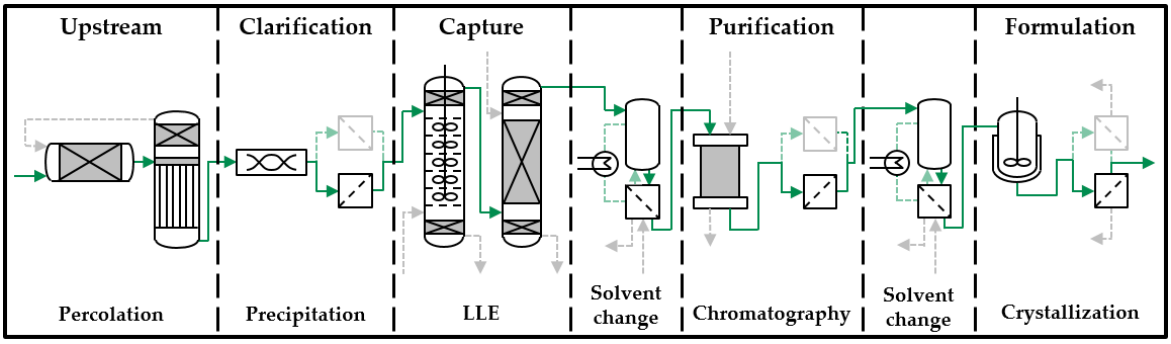

Figure 1. Basic process design for plant-based substances (LLE, liquid-liquid extraction) [8].

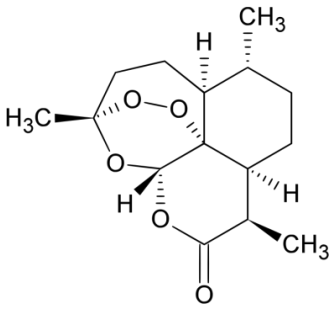

Figure 2. Structure of artemisinin [8].

Crystallization is a typical final purification and isolation step preparing for formulation steps of plant-based or semi-synthetical processes, e.g., artemisinin [11–23]. The crystallization step itself is affected in various ways, based on mechanical and thermodynamic influences, e.g., [24]. The main driving force for crystallization is the solid-liquid equilibrium and, therefore, the solubility of the target component in a system. This solubility is measurable via different methods like the isothermal excess method or the polythermal method, e.g., [25]. Several solvents have been screened for artemisinin [26–29] and there are already described crystallization steps using ethanol, which are used commercially as re-crystallization steps [20]. Due to this, ethanol-mixtures are investigated focusing on target yield and process range. In addition, acetone-water mixtures are also screened based on the good solving properties of the pure solvent for artemisinin [27,28], its high availability, and its usage as the extraction solvent in this process Part 1. This solubility of the target component can be influenced by different approaches like cooling, heating or evaporation. The best controllable and therefore most common crystallization is cooling crystallization [25,30], which is used in this study. Next to solubility, the supersolubility is a vital property of the target component. Primary nucleation leads to a wide and instable particle distribution. To overcome this issue the usage of seed particles is favorable. These seed particles grow in the metastable zone, the area between the solubility and supersolubility curve without primary nucleation [30–33]. For the design space of the crystallization step, information on the metastable zone width (MSZW) is necessary. This information on supersolubility can be obtained via isothermal or polythermal methods and the measured values are affected by several parameters like agitator type, stirring speed or temperature gradient [34–37].

Even though seeding strategies prevent primary nucleation, secondary nucleation like breakage or attrition and agglomeration as counterpart affect the particle distribution. These effects are component-specific, and therefore have to be determined for the chosen artemisinin system [24,31]. Artemisinin forms two polymorphs, which means it grows in different crystal shapes. On the one hand, there is a triclinic, and on the other hand, an orthorhombic crystal shape. Both crystal structures lead to rod-like particles which increase sensibility with regard to breakage, but at temperatures below 130 °C, the orthorhombic configuration is present [38]. The final step for the process design of the crystallization step is the determination of the particle growth and sensitivities based on the operating parameters. The growth of the particles is measurable using several methods and can be separated into methods for a single crystal and for crystal suspensions, e.g., [32]. The simplest and most common approach is the measurement of the desupersaturation curve in a seeded isothermal batch experiment. With information on the concentration and solubility, supersaturation versus time is known, and kinetics can be calculated [32,39]. Alternatives include, for example, the usage of differential scanning calorimetry (DSC) approaches for reduced substances, or direct measurements of kinetics [32,40]. Due to the slow growth of particles, the process time has to be adequately chosen to meet process quality attributes like yield or x_{50} [25]. Based on the controllable parameter influences and sensitivities for the process, quality attributes have to be investigated in order to create a suitable process [41].

Alongside the possibility of creating solids, the crystallization step makes it possible to purify crystals out of a multicomponent solution [21,24]. An integration of the crystallization step provides financial advantages, due to its low operation costs. By integrating the crystallization step into the downstream of artemisinin as a purification step, the composition of the feed solution is essential, because of the influences of side components on solubility and kinetics [15–17,26,32,42,43]. With the shift of the crystallization step to earlier stages, it becomes more affectable by the variability of the side component spectrum, which is a significant factor for plant-based material. For this reason, the critical impurities have to be determined and methods for batch variability of the plant material have to be used [44]. To crystallize artemisinin, those critical side components that increase the solubility have to be removed by preceding unit operations.

In this study, the crystallization of artemisinin is investigated with a focus on process integration into a conceptual process design. Therefore, critical variables, boundaries and sensitivities of the crystallization process are researched, creating a process design space for an organic molecule out of a multicomponent mixture. This includes separation, and tests mechanical and thermodynamic influences with a reduced number of experiments. Furthermore, this study is executed focusing on the modeling of artemisinin crystallization. For this modeling and the crystallization process itself, several effects are separated in order to create a predictive model. The modeling itself will be published in another manuscript, as it would exceed the limits of this paper.

In addition, other process positions within the described process design (see Figure 1) are tested as a combined purification and isolation step in order to reduce the number of process steps and save costs. This is performed with a focus on creating a process design field that enables a controlled crystallization with the aid of modelling. It should contain predictive particle size distribution and ensure the product quality attributes of the product that are desired in a crystallized product [41]. This should, on the one hand, increase the yield of the pharmaceutical substance, and on the other hand, the crystals should become more adjustable for subsequent steps such as filtering, drying and formulation in general, as these subsequent steps are affected by the particle size distribution [25,32,41].

2. Material and Methods

2.1. Raw and Purified Material

Raw *Artemisia annua* L. and purified artemisinin (CfM Oskar Tropitzsch, Markredwitz, Germany) are used for this study. The raw plant material is ground to approximately 1 mm with a Grindomix®

200 knife mill (Retsch GmbH, Haan, Germany). For storage, the plant material and the purified artemisinin are stored at −20 °C to minimize degradation.

2.2. Chemicals

Acetone, ethanol in analytical grade (VWR®, Darmstadt, Germany) and water (Sartorius® arium® pro, Göttingen, Germany) are used as solvent mixtures.

2.3. Crystallization System Screening

Solvent screening is performed with a MKR 13 Thermo Shaker (Hettich Benelux, Geldermalsen, The Netherlands) using 50 mL Falcons® (VWR®, Darmstadt, Germany) and purified artemisinin given in surplus. The mixtures are kept for 3 h at constant temperature before a sample was taken and analyzed.

2.4. Seed Crystals

Seed crystals for the crystallization experiments were obtained from purified artemisinin, which is sieved into the class 100 < x (ferret max.) < 150 µm with. The particle fractions x < 100 µm and x > 150 µm are used in agglomeration and breakage experiments.

2.5. Metastable Zone Width and Crystallization Experiments

Solubility and supersolubility curves are measured with an EXcell 230 (Exner, Recklinghausen, Germany) turbidity sensor and a Conducell 4UxF (Hamilton Company, Reno, NV, USA) conductivity and temperature sensor in a 1 L stirred double jacked vessel. For the experiments, the vessel is filled with 800 mL solvent, resulting in a height to diameter ratio of 1.15 by a ViskoPakt®-rheo 110 (HiTec Zang, Herzogenrath, Germany) with a four-blade axial flow Polytetrafluoroethylene (PTFE) agitator with a blade angle of 45° and 5 cm diameter, positioned 3 cm from the bottom. The temperature of the cooling agent is controlled with a FP50-MA (Julabo, Seelbach, Germany) thermostat. For the metastable zone width (MSZW) experiment, the temperature is lowered until nucleation occurs; afterwards, the solution is heated until the turbidity reaches a constant value. Variables for this are temperature gradient and stirrer speed.

For agglomeration and breakage experiment crystals, 0.2 g of three different sieving fractions are added in a saturated artemisinin solution at 20 °C. Afterwards, the particles are stirred for 2 h at 100 RPM or 400 RPM and the resulting particle size distributions are measured.

The influences on process variables (x_{50}, yield and Space-Time-Yield) are investigated by a full factorial design of experiments comprising start temperature, final temperature, duration of crystallization step and initial supersaturation of the system. For process design experiments the same setup is used as for the measurement of MSZW. The stirring speed is kept constant at 100 RPM and 0.2 g purified artemisinin is used as seed crystals.

After each crystallization experiment the resulting particles are filtered and dried at 60 °C before they are analyzed. The remaining mother liquid is completely evaporated to dryness (IKA®-Werke GmbH & Co. KG, Staufen, Germany) and the resulting artemisinin is dried and sieved for additional experiments.

2.6. Analytics

The analysis of artemisinin is performed by High performance liquid chromatography (HPLC) using an Elite LaChrom® (Hitachi High Technologies America, Schaumburg, IL, USA) device equipped with an Evaporation Light Scatting Detector (ELSD) Alltech® 3300 (Grace®, Columbia, SC, USA). The analytical column is a PharmPrep® RP18 250 mm × 4 mm i.d. by Merck® (Merck KGaA, Darmstadt, Germany) operated at 25 °C. The eluents are acetonitrile (VWR®, Darmstadt, Germany) and water (Sartorius® arium® pro, Göttingen, Germany) 60/40 in isocratic mode at 1 mL/min flow. The injection

volume is 10 µL and all samples are passed through a 0.2 µm syringe filter. The evaporator temperature of the ELSD is set to 36 °C and the air flow is 1.6 mL/min. Calibration is performed with an external standard ordered from CfM Oskar Tropitzsch (Marktredwitz, Germany) over a range from 1 g/L to 0.001 g/L. The basis of the HPLC analysis protocol can be found in Lapkin et al. [45]. It was slightly modified to fit the setup used in this study.

For the H-NMR (Hydrogen Nuclear magnetic resonance) analytics, a Bruker AVANCE III 600 MHz spectrometer (Bruker, Rheinstetten, Germany) is used. It is equipped with a broad-band observe probe head with z-gradient. The samples are completely evaporated to dryness using a rotary evaporator (IKA®-Werke GmbH & Co. KG, Staufen, Germany). The final analyte is then dissolved in deuterated benzene (C_6D_6) for measurement. The H1 spectroscopy of the purified artemisinin is shown with the other spectrums. 1H NMR (600 MHz, C_6D_6, 7.16 ppm): 5.51 (s, 1H), 3.35 (dq, J = 7.3, 5.0 Hz, 1H), 2.23 (ddd, J = 14.5, 13.3, 4.0 Hz, 1H), 1.60 (ddd, J = 14.6, 4.8, 2.9 Hz, 1H), 1.48 (dddd, J = 14.0, 7.0, 4.1, 3.0 Hz, 1H), 1.26 (s, 3H), 1.25–1.20 (m, 2H), 1.12–1.02 (m, 2H), 1.00 (d, J = 7.25 Hz, 3H), 0.92 (ddd, J = 11.1, 11.1, 6.8 Hz, 1H), 0.71–0.62 (m, 1H), 0.60 (d, J = 6.3 Hz, 3H), 0.47–0.37 (m, 2H).

Crystal sizes for agglomeration and breakage experiments are measured using Axiolab A (Zeiss, Oberkochen, Germany) light microscope. The characteristic diameter for the measurements is the ferret max. For the growth experiments the Qicpic (Sympatec GMBH, Clausthal-Zellerfeld, Germany) is used to measure Q3 distributions of the initial and final crystals. As characteristic length, the maximal ferret diameter is chosen.

3. Results and Discussion

Crystallization of artemisinin is the last unit operation step of downstream and the first step of formulation in the purification process. Therefore, yield has to be optimized and the solvents used should be less toxic and easy to remove from the resulting particles. In addition, the particle distribution should be narrow.

3.1. Crystallization of Artemisinin

3.1.1. System Selection

Appropriate choice of solvent system is a vital point for any crystallization process. It defines the solubility of the target component and therefore the possible yield for each crystallization step. A system should comprise the properties of significant concentration gradient of the target component over the temperature and a minor final solubility at low temperatures to obtain a high yield in each crystallization step. Figure 3 shows the results for mixtures of acetone and ethanol mixed with different amounts of water to generate different solubility curves.

Acetone mixtures have, in general, a higher solubility of artemisinin compared to ethanol mixtures, which agrees with previous studies focusing on the pure solvents [23]. Acetone-water 50/50 wt.% and ethanol-water 60/40 wt.% both show a good combination of low concentrations at 4 °C and solubility gradient with change of temperature. Comparing those two systems, acetone-water 50/50 wt.% has a slightly stronger gradient, and ethanol-water 60/40 wt.% has a lower concentration at 4 °C with about 4 g/kg. For the following experiments, ethanol-water 60/40 wt.% is chosen due to the lower final concentration, its known usage for commercial crystallization of artemisinin, and its low toxicity, which is important due to its position as the final Downstream Processing (DSP)step. These reasons are not outweighed by the slightly increased gradient. The ethanol-water 60/40 wt.% system is measured in greater detail, as depicted in Figure 4. The measurements for ethanol-water 60/40 wt.% demonstrate an exponential behavior, resulting in strongly increasing solubility at higher temperatures. 35 °C was taken as the maximum temperature, as it gets unstable at temperatures greater than 40 °C.

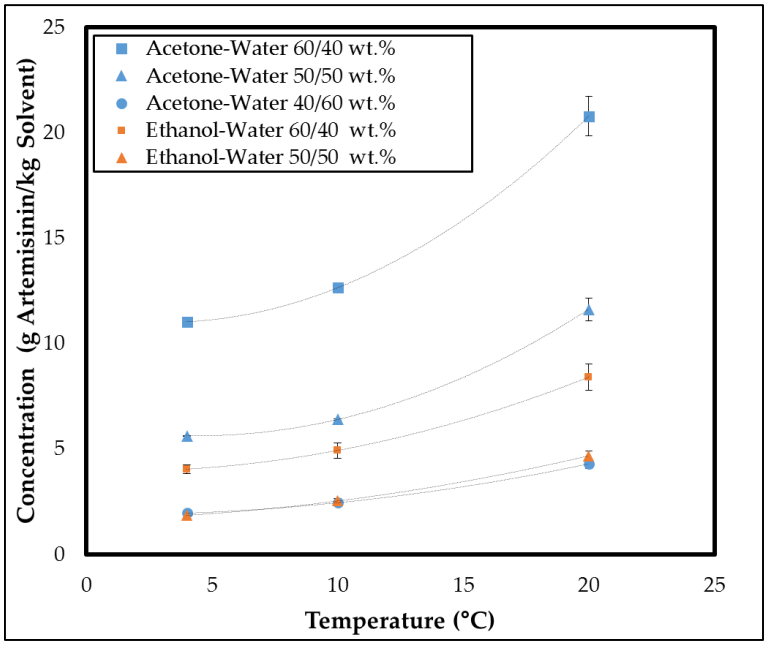

Figure 3. Solubility screening of different acetone-water and ethanol-water mixtures.

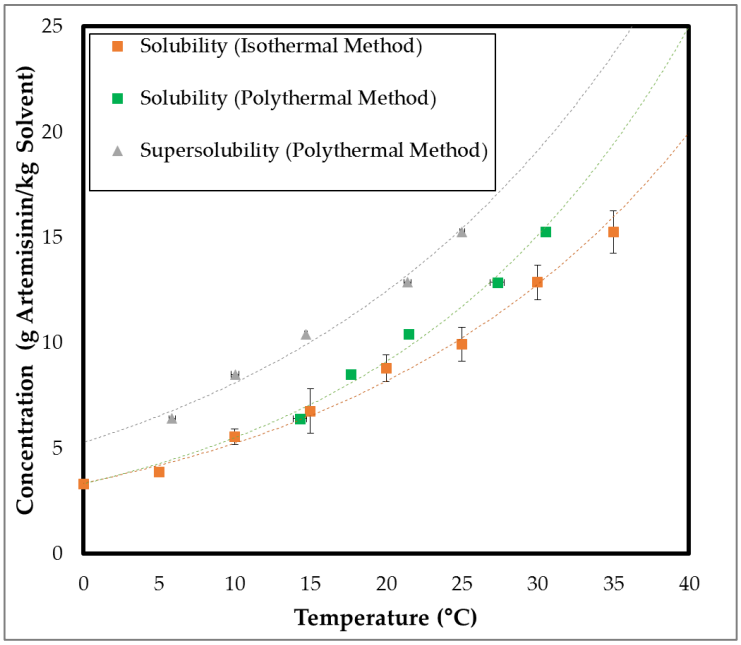

Figure 4. Metastable zone width of artemisinin in ethanol-water 60 wt.%.

3.1.2. Metastable Zone Width

Based on the solubility curve, measured with the isothermal excess method, the MSZW is measured to set the boundaries for the crystallization step. In the literature, the influences of temperature gradient and energy input on the measured nucleation temperature are mentioned [35,36]. To measure the correct values, stirring speed and temperature gradient are investigated for the polythermal method. The results are summarized in Table 1.

Table 1. Influences of stirring speed and temperature gradient on measured metastable zone width.

Variation		Nucleation Temperature (°C)	
Stirring speed (at 1 °C/min)	100 RPM	14.4	±0.4
	200 RPM	15.8	±0.7
	400 RPM	16.4	±0.2
Temperature gradient (at 400 RPM)	0.1 °C/min	20.8	±1.1
	0.5 °C/min	20.6	±0.0
	1.0 °C/min	16.4	±0.2

Based on these experiments, the MSZW should be measured at the highest stirring rate and a low temperature gradient in order to set robust boundaries for the crystallization process. The resulting graphs for solubility (polythermal and isothermal method) and supersolubility are displayed in Figure 4.

Obviously, the resulting solubility curve of the polythermal measurement differs from prior measurements via the isothermal excess method. This difference grows with increasing temperatures. For the process design, the polythermal values are chosen, because they are performed in the crystallization vessel itself and detected with inline measurements. This leads to less handling influence, and therefore less possibility of handling issues. The results for the metastable zone are listed in Table 2.

Table 2. Metastable zone width of artemisinin in 60 wt.% ethanol (MSZW: metastable zone width).

Concentration ($g_{Artemisinin}/kg_{Solvent}$)	MSZW (°C)	
6.4	8.4	±0.7
8.5	7.6	±0.4
10.4	6.8	±0.2
12.9	6.1	±0.7
15.3	5.5	±0.3

At minor concentrations, the MSZW starts with 8.4 °C. In contradiction to this, the difference of nucleation and solubility temperature only covers a range of 5.5 °C at the highest measured concentration. This provides a descending zone, where nucleation does not occur. This leads to a shrinking design space of the crystallization step at higher temperatures.

3.1.3. Agglomeration and Breakage

The particle size distribution of a crystallization process is, on the one hand, affected by the growth of the particles, and on the other hand, by agglomeration, attrition and breakage of the particles. These effects depend on the shear rate, which leads to the assumption that those effects can be separated with different stirrer speeds [24]. At low stirring rates, agglomeration could be assumed to be the predominating effect, and at high shear rates, breakage or attrition should predominantly be present. The following particle size distributions result from high and low stirring rates for different particle sieving classes, which are summarized in Table 3. The effects are measured in a saturated solution at 20 °C. As the "low" stirring rate, 100 RPM is chosen, and 400 RPM is chosen as the "high" stirring rate; each experiment is performed twice, to indicate reproducibility. The initial and final particle size distributions are documented in Figures 5 and 6.

Table 3. Sieving fractions for particles.

Particle Class	Sieving Fraction
Small	$x < 100$ µm
Seed	100 µm $< x <$ 150 µm
Large	150 µm $< x$

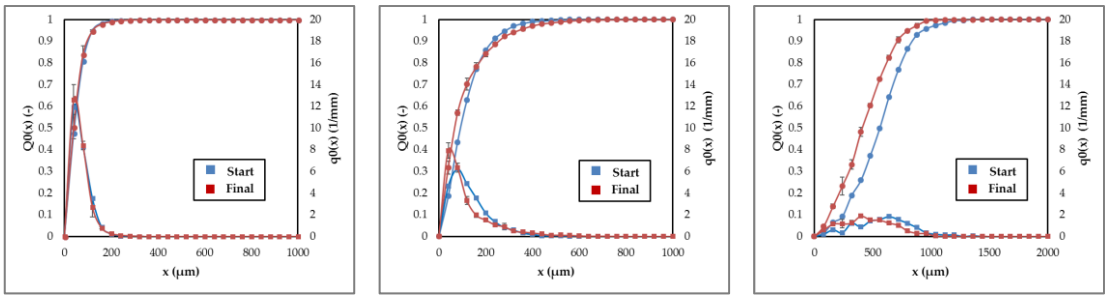

(**a**) (**b**) (**c**)

Figure 5. Agglomeration experiments of different particle fractions: (**a**) small particles, (**b**) seed particles, (**c**) large particles.

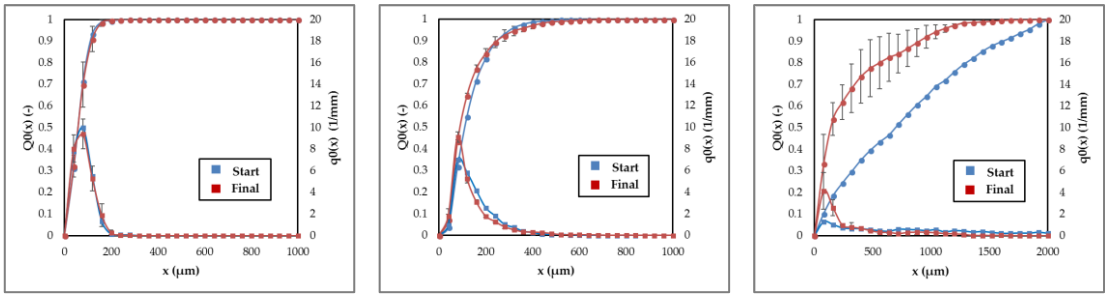

(**a**) (**b**) (**c**)

Figure 6. Breakage experiments of different particle fractions: (**a**) small particles, (**b**) seed particles, (**c**) large particles.

The crystals show no significant changes between start particle size distribution (PSD) and final PSD after 2 h based on agglomeration. There is no detectable shift to larger particle sizes for any of the fractions (see Figure 5a–c). Furthermore, at low stirring speed (100 RPM), attrition and breakage are detectable for large particles (see Figure 5c). As can be seen, the PSD shifts to smaller particle sizes. These experiments demonstrate that agglomeration has no detectable effect on the crystallization of artemisinin. The results for high stirring speed are visualized in Figure 6.

The particle distributions prove, like the previous experiments, that there are no or only minor changes for small and seed particles. For large particles, the effect of breakage is significantly higher than at low stirring rates. Since the probability of breakage increases with greater particle size and agglomeration can be neglected, the process should be operated at low stirring speeds. This would reduce the breakage effects and generate the narrowest particle size distribution for the process.

3.1.4. Process Design

The crystallization process is affected by several thermodynamic influences. While MSZW and mechanical effects of stirring speed have been investigated in the prior sections, influences of start temperature, final temperature, supersaturation and duration have to be investigated, as they are important operating parameters. The results for the examined study are given in the following Table 4. The influences are analyzed regarding their effects on yield, Space-Time-Yield (STY) and x_{50}. The considered yield is based on the thermodynamic limit and follows Equation (1).

$$Y_{TDL} = \frac{C_{Start,measured} - C_{Final,measured}}{C_{Start,measured} - C_{Final.\ theoretical}} \quad (1)$$

Table 4. Design of experiments for growth experiments (STY: Space-Time-Yield; TDL: Thermodynamic limit).

	Pattern	$S_{Initial}$ (−)	T_{Start} (°C)	T_{Final} (°C)	Duration (min)	x_{50} (µm)		$Yield_{TDL}$ (−)	STY (g/(L·h))
1	0000	0.175	25	5	180	221.19	±33.23	0.89	1.17
2	−−−+	0.1	30	10	120	233.14	±4.16	0.80	2.66
3	−+−−	0.1	20	10	240	558.85	±9.46	0.65	1.26
4	0000	0.175	25	5	180	313.04	±27.12	0.83	1.30
5	0000	0.175	25	5	180	258.15	±21.90	0.87	1.22
6	+−++	0.25	30	0	120	226.17	±15.17	0.90	1.77
7	−+−+	0.1	20	10	120	279.55	±10.63	0.61	2.62
8	+−+−	0.25	30	0	240	201.55	±5.36	0.93	0.78
9	+−−−	0.25	30	10	240	207.27	±27.87	0.86	1.26
10	−++−	0.1	20	0	240	294.79	±45.22	0.85	0.77
11	−−+−	0.1	30	0	240	261.51	±39.31	0.92	0.79
12	−+++	0.1	20	0	120	161.75	±2.00	0.84	1.58
13	−−++	0.1	30	0	120	211.70	±14.06	0.88	1.79
14	+−−+	0.25	30	10	120	212.82	±30.67	0.85	2.61
15	++−+	0.25	20	10	120	308.01	±36.33	0.68	2.56
16	++−−	0.25	20	10	240	249.53	±47.18	0.82	1.12
17	+++−	0.25	20	0	240	188.54	±4.04	0.88	0.78
18	−−−−	0.1	30	10	240	224.40	±16.11	0.84	1.24
19	++++	0.25	20	0	120	160.28	±5.93	0.83	1.69

To obtain information about reproducibility, the center points are performed 3 times. The results for volume-based particle size sum distribution and reduction of concentration for the center points (CP) are plotted in the following Figure 7a,b.

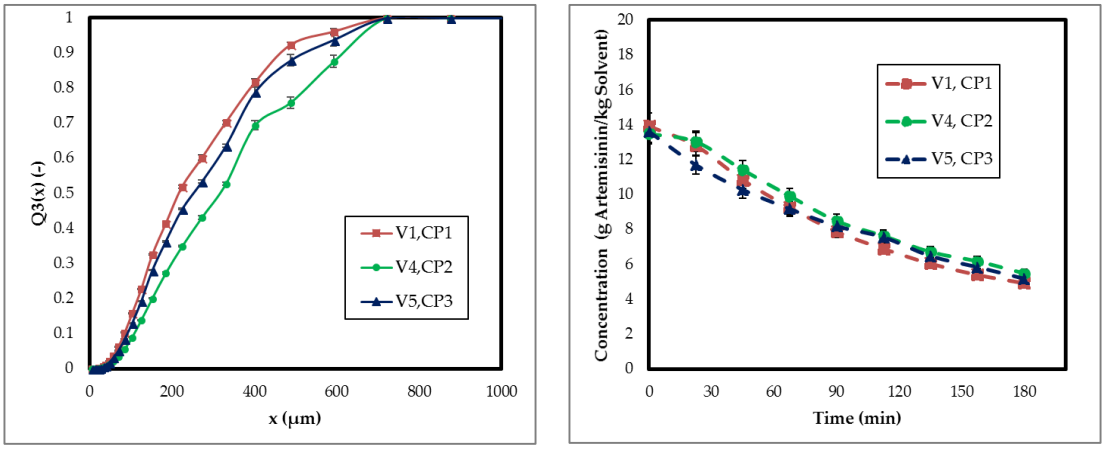

(**a**) (**b**)

Figure 7. Process reproducibility: (**a**) particle size distribution, (**b**) concentration profile. (CP: Center point).

The figure points out a slight variance in particle size distributions and the concentration curves. While the particle size distribution of CP2 differs from CP1 and CP3, it had the slowest reduction of concentration during the beginning of the crystallization. The maximal measured concentration difference of the center points is detectable at the beginning of the processes at 25 min, with a difference of about 1.6 g/kg, which decreases to 0.45 g/kg until the end of the process. Based on the results of the experiments, the center points show a good reproducibility regarding concentration measurement, and the particle size differs slightly.

Significances and main effects on the different process variants are summarized in Figures 8–10, comprising a tornado sensitivity diagram (named pareto chart, using the software Minitab 17™ (Minitab Inc., State Collage, PA, USA)) and a main effect plot. Based on this, only significant parameters are investigated regarding their effect on the process variables.

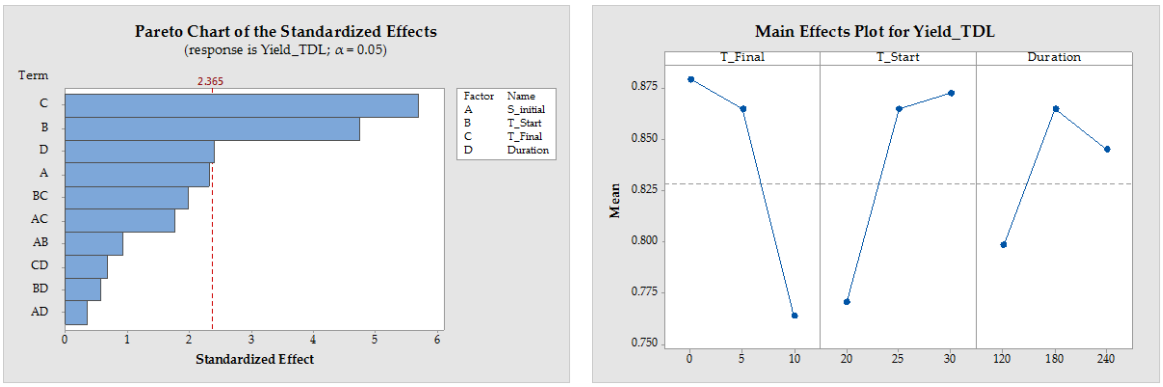

(**a**) (**b**)

Figure 8. Influences on $Yield_{TDL}$: (**a**) significances and (**b**) main effects (TDL: Thermodynamic limit).

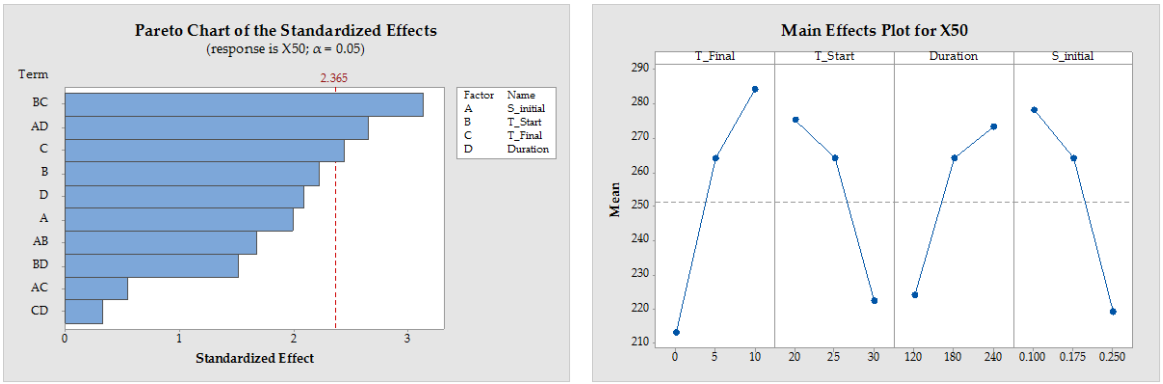

(**a**) (**b**)

Figure 9. Influences on x_{50}: (**a**) significances and (**b**) main effects.

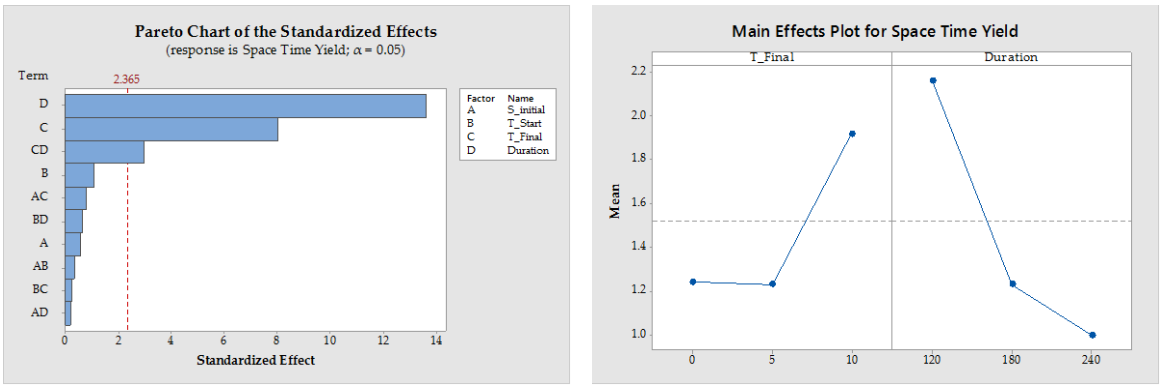

(**a**) (**b**)

Figure 10. Influences on Space-Time-Yield: (**a**) significances and (**b**) main effects.

The yield is strongly affected by the starting and the final temperature. Figure 8a also proves a slight significance of the duration of the crystallization step. The main effect plot (Figure 8b) depicts that for high differences of starting and final temperature the yield maximizes, but with the solubility curve in mind, further cooling is not rational. In addition, higher starting temperatures and therefore higher starting concentrations are also limited due to the instability of the system. The duration main effect plot indicates that the crystallization should exceed 120 min for higher yields, but as Figure 8b shows, the highest duration itself does not necessarily lead to the highest yield.

The x_{50}-value is mainly affected by the interaction of the start and final temperature and, in addition, by the interaction of initial supersaturation and the duration of the crystallization

experiment. Furthermore, Figure 9a shows that the final temperature itself has an influence on the medium particle size. The main effect plot for x_{50} proves that low temperature differences create greater particles in comparison to large differences. In addition, highly supersaturated and long experiments create larger particles than low supersaturated and short experiments. To increase the medium particle length, it is favorable to have a high initial supersaturation and an increased process duration. In contrast, the temperature difference should be small.

Space-Time-Yield of the process is mainly affected by the duration of the process, final temperature and interaction of those process parameters. Figure 10b also concludes that long processes generate a significantly worse STY and that a minimum temperature of 10 °C should be used.

This study applied on these characteristic numbers (yield, STY, x_{50}) proves that even though the average yield is reduced with higher final temperatures, enhanced cooling is not necessary to create a suitable process. Due to the lower solubility change after 10 °C, further cooling does not increase the STY of the process. From a processing point of view, the duration should be as short as possible, as the STY already showed. In contradiction to STY, the shortened process time negatively affects the growth and the yield of the process. Focusing on high yield, the starting temperature should be as high as possible, due to the exponential increasing solubility at high concentrations, but also affects the medium crystal size negatively. This study also emphasizes that crystallization becomes a time-consuming unit operation, if high yields and large crystals should be achieved. Initial supersaturation variation also indicates that high initial supersaturations do not enhance yield or STY, but decrease the medium crystal size, which affects solid-liquid separation and drying.

3.2. Process Integration of Crystallization Step

The conceptual process design for artemisinin, mentioned in Figure 1, uses crystallization as an isolation step of the target component in preparation for the formulation steps, while it neglects the capability of purifying the target component. However, any reduction in the number of separation units provides a major possibility to save costs. Because of this, a process integration study for the crystallization unit as a purifying and formulation step is examined. The different possible process points are summarized in Figure 11.

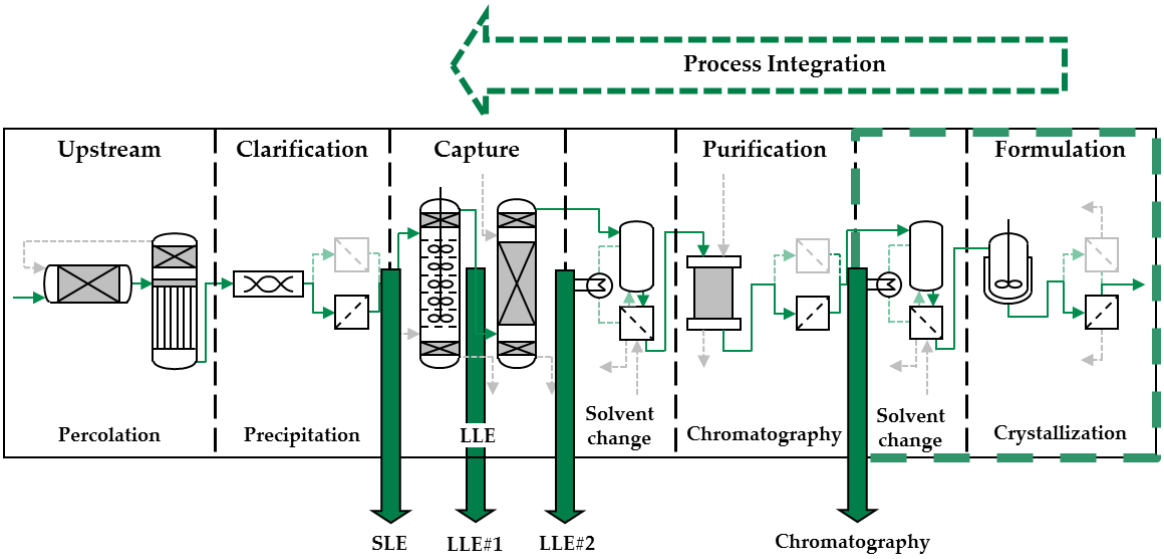

Figure 11. Possible process points for crystallization step. (SLE: Solid-liquid extraction).

Cooling to −20 °C of the SLE (Solid-liquid extraction)-extract and LLE#1-raffinate in ethanol-water 60/40 wt.% does not lead to crystals. In contradiction to these results, it is possible to create crystals out of the LLE#2-raffinate and the chromatographic solution. This leads to the assumption that the critical side components, which drastically increase the solubility of the target component, are removed

by the LLE#2 step. The results for the chromatography fraction and the LLE#2-raffinate are shown in Figure 12.

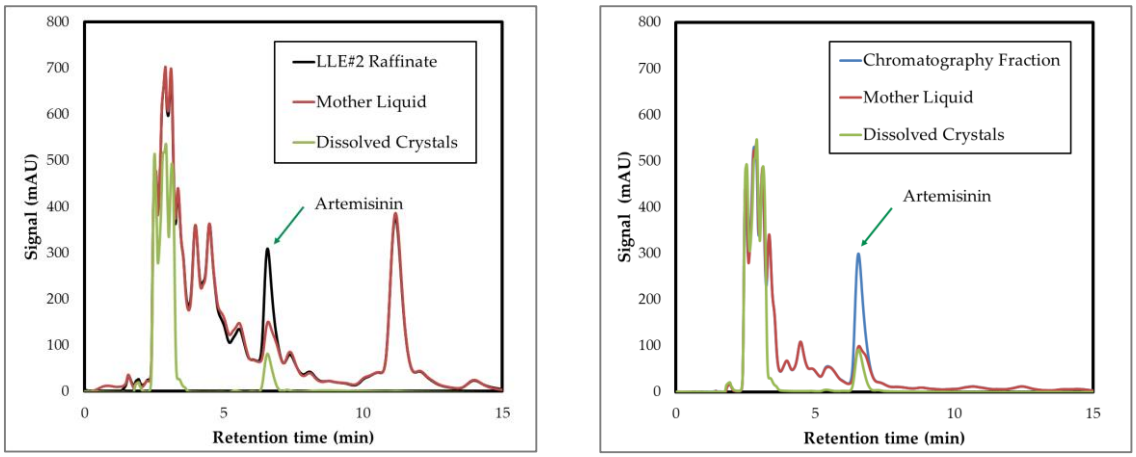

(**a**) (**b**)

Figure 12. HPLC analysis of crystallization experiments of (**a**) LLE#2-raffinate and (**b**) chromatography fraction. (HPLC: High performance liquid chromatography).

Both experiments prove a selective reduction of artemisinin with a high purity of the dissolved crystals. This leads to the conclusion that the chromatographic step could be substituted by the crystallization step. An additional H-NMR analysis (see Figure 13) is performed to control these results from HPLC analysis, focusing on purity. As a reference for the measured solutions, a purified commercial artemisinin substance is used.

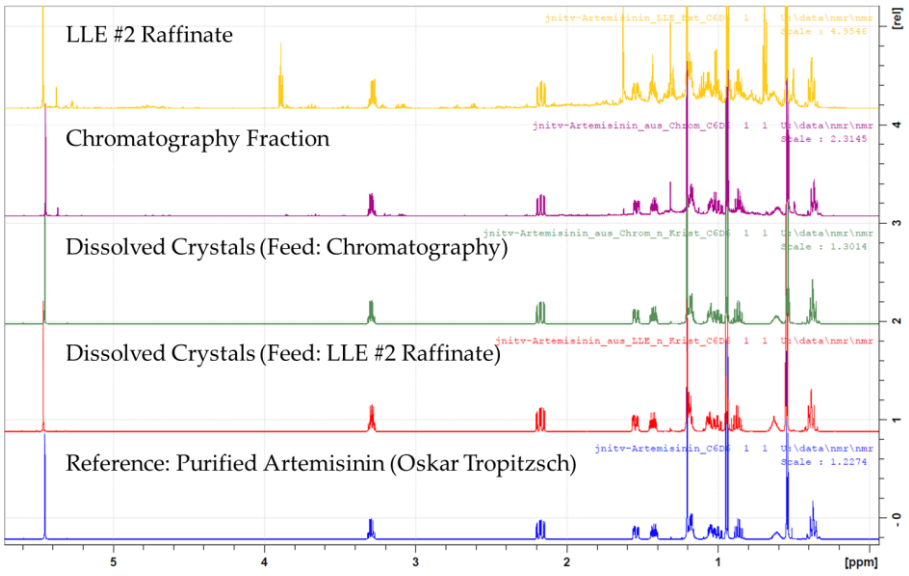

Figure 13. H-NMR measurement of process points. (HNMR: Hydrogen Nuclear magnetic resonance).

The H-NMR analysis proves that the purities of both dissolved crystal solutions are higher than the purity of the chromatography fraction. The LLE#2-raffinate has the lowest purity, containing the most signals differing from the reference material. These measurements support the HPLC analysis results. Hence, the quality of the product is confirmed, the chromatographic step is not essential with regard to purity (as proven experimentally, see Figure 13) and can be substituted within the total process by a cooling crystallization step, as long as critical side components that strongly affect the

crystallization are removed by an optimized LLE. This would reduce the costs (see Part I) by about 40%. The resulting chromatography reduced process is visualized in Figure 14.

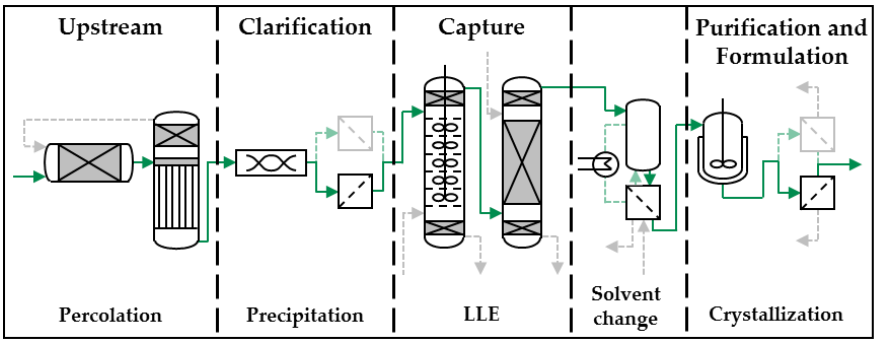

Figure 14. Reduced purification process of artemisinin.

One solvent change step and the chromatographic purification step can be excluded from the total process. This leads to only three orthogonal separation units being necessary to purify artemisinin. The influences of the side components on growth kinetics, on the other hand, must be investigated more closely in future, as well. This will result in the final statement on cost reduction, due to possible shifts in solubility and growth kinetics caused by side components. In addition, appropriate reduction of critical side components for early crystallization without losing yield have to be solved by optimization of the LLE-steps (see Part II).

4. Conclusions

This study comprises a systematic integration of the crystallization step in a purification process from *Artemisia annua* L. Several aspects containing metastable zone width, agglomeration, and breakage are researched. In addition, sensitivities of different product quality attributes and their influences are investigated at pilot scale. It is demonstrated that the detected metastable zone width is influenced by temperature gradient and stirring speed. To set robust boundaries, the smallest detected MSZW is chosen for the process. On the one hand agglomeration does not affect the crystallization of artemisinin, on the other hand breakage and attrition are vital effects even for the seed crystals at high stirring rates. Therefore, a low stirring rate is useful to reduce the mentioned effects and create narrow particle distributions. The process design experiments show no single solution to optimize the crystallization process. Based on the different product quality attributes and characteristic performance numbers, the process parameters have to be adjusted appropriately as proposed. To create the optimized process, the quality attributes and/or characteristic process performance numbers have to be weighted and the resulting multi parameter problem can be solved adequately. Hence, no processes reach a yield greater than 95%, an industrial process needs recycling of the remaining mother liquid, a multi-step crystallization which can be designed and optimized with the aid of the modelling approach [24].

In addition, a process integration study has been performed for the crystallization step. The results display the possibility of substituting the chromatographic step. This is accomplished without loss of product purity with an optimized LLE in combination with crystallization. This substitution has a major impact on production costs and would reduce them by around 40% by using crystallization as a combined purification and isolation step preparing the final formulation. However, effects on kinetics and solubility caused by remaining side components need to be further investigated, as these may reduce the potential for cost reduction through yield losses. Moreover, the natural variability of plant material, which leads to different side component spectra, can affect the downstream process and is considered in conceptual process design [44]. If the critical side components are removed early, as in this study, process integration of the crystallization step provides an enormous potential for cost savings.

Author Contributions: M.J.H. conceived and designed the crystallization experiments as well as wrote the paper. M.S. designed the solid-liquid extraction experiments. A.S. designed the liquid-liquid extraction experiments and F.M. designed the chromatographic experiments. J.S. substantively revised the work and contributed the materials. J.S. is responsible for conception and supervision.

Funding: The authors want to thank the Bundesministerium für Wirtschaft und Energie (BMWi), especially M. Gahr (Projektträger FZ Jülich), for funding this scientific work. We also acknowledge the financial support obtained from the Deutsche Forschungsgemeinschaft (DFG) in Bonn, Germany (project Str 586/4-2).

Acknowledgments: We gratefully acknowledge the support of the ITVP lab team. In addition, we want to thank J. Namyslo from the IOC for performing the H-NMR analysis and the PuK for performing the QicPic measurements. Special thanks are also addressed to Sebastian Weismann and Thomas Weber for excellent laboratory work and fruitful discussions.

Conflicts of Interest: The authors declare no conflict of interest.

Abbreviations

c	Concentration in the liquid phase, g/kg
q_0	Number-based particle size density distribution, 1/mm
Q_0	Number-based particle size sum distribution, -
q_3	Volume-based particle size density distribution, 1/mm
Q_3	Volume-based particle size sum distribution, -
S	Supersaturation, -
T	Temperature, °C
x	Particle length, µm
x_{50}	Median value of particle size distribution
Y	Yield, -
ELSD	Evaporation Light Scattering Detector
HPLC	High performance liquid chromatography
H-NMR	Hydrogen Nuclear magnetic resonance
MSZW	Metastable zone width
RPM	Rounds per minute
STY	Space-Time-Yield

References

1. Kassing, M.; Jenelten, U.; Schenk, J.; Hänsch, R.; Strube, J. Combination of rigorous and statistical modeling for process development of plant-based extractions based on mass balances and biological aspects. *Chem. Eng. Technol.* **2012**, *35*, 109–132. [CrossRef]
2. Ditz, R.; Gerard, D.; Hagels, H.; Igl, N.; Schäffler, M.; Schulz, H.; Stürtz, M.; Tegtmeier, M.; Treutwein, J.; Strube, J.; et al. *Phytoextracts. Proposal Towards a New Comprehensive Research Focus*; ProcessNet-Subject Division Plant Based Extracts—Products and Processes: Frankfurt, Germany, 2017.
3. Both, S. *Systematische Verfahrensentwicklung Für Pflanzlich Basierte Produkte im Regulatorischen Umfeld*; Shaker: Aachen, Germany, 2015; ISBN 978-3-8440-3727-2.
4. Koudous, I. *Stoffdatenbasierte Verfahrensentwicklung zur Isolierung von Wertstoffen aus Pflanzenextrakten*, 1st ed.; Shaker: Herzogenrath, Germany, 2017; ISBN 978-3-8440-5271-8.
5. Koudous, I.; Both, S.; Gudi, G.; Schulz, H.; Strube, J. Process design based on physicochemical properties for the example of obtaining valuable products from plant-based extracts. *C. R. Chim.* **2014**, *17*, 218–231. [CrossRef]
6. Sixt, M.; Koudous, I.; Strube, J. Process design for integration of extraction, purification and formulation with alternative solvent concepts. *C. R. Chim.* **2016**, *19*, 733–748. [CrossRef]
7. Sixt, M.; Strube, J. Systematic and model-assisted evaluation of solvent based- or pressurized hot water extraction for the extraction of artemisinin from *Artemisia annua* L. *Processes* **2017**, *5*, 86. [CrossRef]
8. Sixt, M.; Schmidt, A.; Mestmäcker, F.; Huter, M.J.; Uhlenbrock, L.; Strube, J. Systematic and model-assisted process design for the extraction and purification of Artemisinin from *Artemisia annua* L.—Part I: Conceptual process design and cost estimation. *Processes* **2018**, *6*, 161. [CrossRef]

9. Schmidt, A.; Sixt, M.; Huter, M.; Mestmäcker, F.; Strube, J. Systematic and model-assisted process design for the extraction and purification of Artemisinin from *Artemisia annua* L.—Part II: Model-based design of agitated and packed columns for multistage extraction and scrubbing. *Processes* **2018**, *6*, 179. [CrossRef]
10. Mestmäcker, F.; Schmidt, A.; Huter, M.; Sixt, M.; Strube, J. Systematic and model-assisted process design for the extraction and purification of Artemisinin from *Artemisia annua* L.—Part III: Chromatographic Purification. *Processes* **2018**, *6*, 180. [CrossRef]
11. Kumar, S.; Gupta, S.K.; Singh, D.; Gupta, M.M.; Jain, D.C.; Kahol, A.P.; Kahuja, S.P.S.; Ram, G. Process for Isolating Artemisinin from *Artemisia annua*. U.S. Patent 6,685,972, 3 March 2004.
12. Liu, N.Q.; Schuehly, W.; Von Freyhold, M.; Van der Kooy, F. A novel purification method of artemisinin from *Artemisia annua*. *Ind. Crops Prod.* **2011**, *34*, 1084–1088. [CrossRef]
13. Harjo, B.; Wibowo, C.; Ng, K.M. Development of natural product manufacturing processes. *Chem. Eng. Res. Des.* **2004**, *82*, 1010–1028. [CrossRef]
14. ElFeraly, F.; Elsohly, H.N. Method for the Isolation of Artemisinin from *Artemisa annua*. U.S. Patent 4,952,603, 28 August 1990.
15. Malwade, C.R.; Qu, H.; Rong, B.-G.; Christensen, L.P. Conceptual process synthesis for recovery of natural products from plants: A case study of artemisinin from *Artemisia annua*. *Ind. Eng. Chem. Res.* **2013**, *52*, 7157–7169. [CrossRef]
16. Malwade, C.R.; Qu, H.; Rong, B.-G.; Christensen, L.P. Purification of artemisinin from quercetin by anti-solvent crystallization. *Front. Chem. Sci. Eng.* **2013**, *7*, 72–78. [CrossRef]
17. Malwade, C.R.; Buchholz, H.; Rong, B.-G.; Qu, H.; Christensen, L.P.; Lorenz, H.; Seidel-Morgenstern, A. Crystallization of artemisinin from chromatography fractions of *Artemisia annua* extract. *Org. Process Res. Dev.* **2016**, *20*, 646–652. [CrossRef]
18. Lévesque, F.; Seeberger, P.H. Continuous-flow synthesis of the anti-malaria drug artemisinin. *Angew. Chem. Int. Ed.* **2012**, *51*, 1706–1709. [CrossRef] [PubMed]
19. Turconi, J.; Griolet, F.; Guevel, R.; Oddon, G.; Villa, R.; Geatti, A.; Hvala, M.; Rossen, K.; Göller, R.; Burgard, A. Semisynthetic artemisinin, the chemical path to industrial production. *Org. Process Res. Dev.* **2014**, *18*, 417–422. [CrossRef]
20. Tu, Y. *From Artemisia annua L. to Artemisinins: The Discovery and Development of Artemisinins and Antimalarial Agents*; Elsevier Science: San Diego, CA, USA, 2017; ISBN 978-0-12-811655-5.
21. Lorenz, H. Purification by crystallization. In *Crystallization: Basic Concepts and Industrial Applications*; Beckmann, W., Ed.; Wiley-VCH Verlag GmbH & Co. KGaA: Weinheim, Germany, 2013; pp. 127–148, ISBN 978-3-527-32762-1.
22. Chemat, F.; Strube, J. *Green Extraction of Natural Products: Theory and Practice*, 1st ed.; Wiley-VCH: Weinheim, Germany, 2015.
23. Strube, J.; Grote, F.; Josch, J.P.; Ditz, R. Process development and design of downstream processes. *Chem. Ing. Tech.* **2011**, *83*, 1044–1065. [CrossRef]
24. Lucke, M.; Koudous, I.; Sixt, M.; Huter, M.J.; Strube, J. Integrating crystallization with experimental model parameter determination and modeling into conceptual process design for the purification of complex feed mixtures. *Chem. Eng. Res. Des.* **2018**, *133*, 264–280. [CrossRef]
25. Beckmann, W. *Crystallization. Basic Concepts and Industrial Applications*; Wiley-VCH Verlag GmbH & Co. KGaA: Weinheim, Germany, 2013; ISBN 978-3-527-32762-1.
26. Qu, H. Chromatography-crystallization hybrid process for artemisinin purification from *Artemisia annua*. *Chem. Eng. Technol.* **2010**, *33*, 791–796. [CrossRef]
27. Lapkin, A.A.; Peters, M.; Greiner, L.; Chemat, S.; Leonhard, K.; Liauw, M.A.; Leitner, W. Screening of new solvents for artemisininextraction process using ab initio methodology. *Green Chem.* **2010**, *12*, 241–251. [CrossRef]
28. Liu, Y.; Lü, H.; Pang, F. Solubility of artemisinin in seven different pure solvents from (283.15 to 323.15) K. *J. Chem. Eng. Data* **2009**, *54*, 762–764. [CrossRef]
29. Wang, L.-H.; Song, Y.-T.; Chen, Y.; Cheng, Y.-Y. Solubility of artemisinin in ethanol + water from (278.2 to 343.2) K. *J. Chem. Eng. Data* **2007**, *52*, 757–758. [CrossRef]
30. Hofmann, G.; Beckmann, W. *Kristallisation in der Industriellen Praxis*; Wiley-VCH: Weinheim, Germany, 2004; ISBN 978-352-760-273-5.

31. Wieckhusen, D. Development of batch crystallizations. In *Crystallization: Basic Concepts and Industrial Applications*; Beckmann, W., Ed.; Wiley-VCH Verlag GmbH & Co. KGaA: Weinheim, Germany, 2013; pp. 187–202, ISBN 978-3-527-32762-1.
32. Myerson, A.S. *Handbook of Industrial Crystallization*, 2nd ed.; Butterworth-Heinemann: Boston, MA, USA, 2002; ISBN 978-008-053-351-3.
33. Mullin, J.W. *Crystallization*, 4th ed.; Butterworth-Heinemann: Oxford, UK, 2001; ISBN 978-075-064-833-2.
34. Kim, K.-J.; Mersmann, A. Estimation of metastable zone width in different nucleation processes. *Chem. Eng. Sci.* **2001**, *56*, 2315–2324. [CrossRef]
35. Liu, J.; Svärd, M.; Rasmuson, Å.C. Influence of agitation on primary nucleation in stirred tank crystallizers. *Cryst. Growth Des.* **2015**, *15*, 4177–4184. [CrossRef]
36. Bogacz, W.; Wójcik, J. The metastable zone of aqueous solutions. *Chemik* **2014**, *68*, 198–201.
37. Mohan, R.; Lorenz, H.; Myerson, A.S. Solubility measurement using differential scanning calorimetry. *Ind. Eng. Chem. Res.* **2002**, *41*, 4854–4862. [CrossRef]
38. Chan, K.-L.; Yuen, K.-H.; Takayanagi, H. Polymorphism of artemisinin from *Artemisia annua*. *Phytochemistry* **1997**, *46*, 1209–1214. [CrossRef]
39. Glade, H.; Ilyaskarov, A.M.; Ulrich, J. Determination of crystal growth kinetics using ultrasonic technique. *Chem. Eng. Technol.* **2004**, *27*, 736–740. [CrossRef]
40. Mohan, R.; Boateng, K.A.; Myerson, A.S. Estimation of crystal growth kinetics using differential scanning calorimetry. *J. Cryst. Growth* **2000**, *212*, 489–499. [CrossRef]
41. Variankaval, N.; Cote, A.S.; Doherty, M.F. From form to function: Crystallization of active pharmaceutical ingredients. *AIChE J.* **2008**, *54*, 1682–1688. [CrossRef]
42. Josch, J.P.; Both, S.; Strube, J. Characterization of feed properties for conceptual process design involving complex mixtures, such as natural extracts. *FNS* **2012**, *3*, 836–850. [CrossRef]
43. Suberu, J.O.; Yamin, P.; Leonhard, K.; Song, L.; Chemat, S.; Sullivan, N.; Barker, G.; Lapkin, A.A. The effect of O-methylated flavonoids and other co-metabolites on the crystallization and purification of artemisinin. *J. Biotechnol.* **2014**, *171*, 25–33. [CrossRef] [PubMed]
44. Sixt, M.; Strube, J. Systematic design and evaluation of an extraction process for traditionally used herbal medicine on the example of hawthorn (*Crataegus monogyna* Jacq.). *Processes* **2018**, *6*, 73. [CrossRef]
45. Lapkin, A.A.; Walker, A.; Sullivan, N.; Khambay, B.; Mlambo, B.; Chemat, S. Development of HPLC analytical protocols for quantification of artemisinin in biomass and extracts. *J. Pharm. Biomed. Anal.* **2009**, *49*, 908–915. [CrossRef] [PubMed]